Tissue Eng Regen Med (2018) 15(2):131–143
https://doi.org/10.1007/s13770-017-0100-z

Online ISSN 2212-5469
Print ISSN 1738-2696

ORIGINAL ARTICLE

Preparation of Drug Eluting Natural Composite Scaffold Using Response Surface Methodology and Artificial Neural Network Approach

Shailendra Singh Shera[1] · Shraddha Sahu[1] · Rathindra Mohan Banik[1]

Received: 8 September 2017 / Revised: 9 November 2017 / Accepted: 19 November 2017 / Published online: 16 January 2018

Abstract Silk fibroin/xanthan composite was investigated as a suitable biomedical material for controlled drug delivery, and blending ratios of silk fibroin and xanthan were optimized by response surface methodology (RSM) and artificial neural network (ANN) approach. A non-linear ANN model was developed to predict the effect of blending ratios, percentage swelling and porosity of composite material on cumulative percentage release. The efficiency of RSM was assessed against ANN and it was found that ANN is better in optimizing and modeling studies for the fabrication of the composite material. *In-vitro* release studies of the loaded drug chloramphenicol showed that the optimum composite scaffold was able to minimize burst release of drug and was followed by controlled release for 5 days. Mechanistic study of release revealed that the drug release process is diffusion controlled. Moreover, during tissue engineering application, investigation of release pattern of incorporated bioactive agent is beneficial to predict, control and monitor cellular response of growing tissues. This work also presented a novel insight into usage of various drug release model to predict material properties. Based on the goodness of fit of the model, Korsmeyer–Peppas was found to agree well with experimental drug release profile, which indicated that the fabricated material has swellable nature. The chloramphenicol (CHL) loaded scaffold showed better efficacy against gram positive and gram negative bacteria. CHL loaded SFX55 (50:50) scaffold shows promising biocomposite for drug delivery and tissue engineering applications.

Keywords Artificial neural network · Response surface methodology · Controlled drug delivery · Silk fibroin/xanthan

1 Introduction

Silk fibroin (SF) is the widely used biomaterial due to its favorable biological compatibility, biodegradability, and mechanical strength [1]. In recent years, SF has been blended with polysaccharides such as chitosan, hyaluronic acid, alginate and k-carragenan for various biomedical applications [2–5]. The mixing of polysaccharide to SF imparts a certain degree of elasticity, softness, and hydrophilicity to the blended material. Moreover, polysaccharide provides nutritive material for cell growth and some level of roughness to the scaffold which aids in better cell attachment and growth [2]. Xanthan gum (Xa), an anionic polysaccharide has wide use in food and cosmetic industries and pharmaceutical industries but finds limited application in drug delivery and tissue engineering

Electronic supplementary material The online version of this article (https://doi.org/10.1007/s13770-017-0100-z) contains supplementary material, which is available to authorized users.

✉ Rathindra Mohan Banik
rmbanik@gmail.com

Shailendra Singh Shera
shailendra.shera@gmail.com

[1] Bioprocess Technology Laboratory, School of Biochemical Engineering, Indian Institute of Technology (Banaras Hindu University), Varanasi, Lanka, Varanasi, Uttar Pradesh 221005, India

due to its low mechanical stability, slow dissolution and substantial swelling in biological fluids [6]. Blending of silk fibroin with xanthan is expected to control the excessive swelling of xanthan, and modulates porosity and release behavior of incorporated drugs and provides robustness to composite scaffold. It has been reported that anionic polysaccharides are suitable biomaterial for bone tissue engineering due to their ability to provide a biomimetic condition for pre-osteoblast cell differentiation and to regulate the mineralization [3]. Therefore, anionic nature of xanthan is expected to increase the functionality of silk fibroin/Xanthan (SF/Xa) composite towards drug delivery and tissue engineering.

Newer methodologies are employed towards development and improvement of devices for more efficient and effective processing of biomaterials [7]. The use of computer-based optimization techniques simplifies the search of optimal design parameter for biomaterial development by reducing several experimental run and development time. Response Surface Methodology (RSM) is one such technique widely used for defining the relationship between various process parameters and responses with the various desired criteria and searching the significance of these process parameters on the coupled responses [8]. However, RSM cannot be applied to optimize non-linear system frequently encountered in material research where small variation in composition, processing parameter or experimental parameter can result in large variation in properties and consequently the output dependent on those properties. Since prediction and optimization capability of RSM is based on simple first or second order polynomial equation, it is unable to capture non-linear behavior and can give a poor estimation of drug release from the polymeric material [9]. Artificial Neural Network (ANN) can overcome the limitation of RSM in predicting non-linear system. ANN is a model-independent method which can efficiently capture the nonlinearity in responses associated with drug release from polymer matrices [10].

The material composition of scaffold has direct bearing on drug release and *invivo* performances. Drug release models combined with experiments give useful insight into physical properties and underlying mass transfer phenomenon affecting release from scaffold. Investigation of release kinetics is significant because concentration of delivered species affects tissue interactions and cellular response. Moreover, mathematical modeling approaches provide useful insight regarding the optimized design parameter at an early stage of scaffold development [11, 12] and can give firsthand estimation of material properties.

The novelty factor of present work is optimization of blending ratios, swelling and porosity using combinatorial approach of RSM and ANN for the fabrication of biopolymeric composite material from silk fibroin and xanthan solution. The utility of xanthan as a natural polymeric blend with silk fibroin for the preparation of scaffold for controlled drug delivery was evaluated. The present work also showed the advantage of ANN over RSM to predict non-linear material behavior encountered in the development of material for tissue engineering and pharmaceutical applications. This study attempted to correlate the effect of blending composition, swelling, and porosity on cumulative percentage drug release. This work also presents a new insight, how various drug release model can be applied to the firsthand account of material properties solely from *invitro* drug release studies?

2 Materials and methods

2.1 Preparation of aqueous silk fibroin solution

Aqueous silk fibroin (SF) solution was prepared with slight modification of the previously described protocol [13]. Briefly, whole cocoons were cut into small pieces, rinsed thoroughly and boiled thrice in an aqueous solution of 1% $NaHCO_3$ for 30 min to extract glue like substance sericin protein and wax. The extracted silk fiber was rinsed thoroughly and allowed to dry at room temperature for 2 days. The dried silk fiber was dissolved in 9.3 M aqueous Lithium Bromide (LiBr) solution, poured into the dialysis tube (MWCO 12–14 K, Himedia), ends were closed by closure clip and dialyzed against distilled water for 3 days to remove LiBr from fibroin solution. After dialysis, this solution was centrifuged at 8000 rpm for 10 min to yield a clear, amber colored solution. The final concentration of aqueous silk solution was 7%wt which was determined by weighing the remaining solids after drying.

2.2 Preparation of xanthan solution

A 0.3%wt xanthan solution (Xa) was prepared by dissolving xanthan powder in distilled water and was kept in the refrigerator for further experiments.

2.3 Preparations of silk fibroin/xanthan blend

7% Silk fibroin solution and 0.3% xanthan solution were mixed in the ratio of 80:20, 50:50 and 20:80 blended solution was sonicated at 0.5 cycle with 50% amplitude for 30 s using Ultrasonicator (Hielscher, Germany) to achieve homogenous mixing of the two components.

2.4 Fabrication of composite scaffold by freeze drying

The blended solutions of different ratios were cast in molds and frozen at − 50 °C for 6 h followed by lyophilization of frozen sample at − 50 °C for 48 h at vacuum of 0–2 mm Torr to prepare SFX82 (80:20), SFX55 (50:50) and SFX28 (80:20) porous scaffolds. The optimization was done using statistical approach of Response Surface Methodology (RSM) and Artificial Neural Network (ANN). For statistical optimization using RSM, defining the higher (80:20), middle (50:50), and lower range (20:80) is a prerequisite for creation of design matrix (Table 3) by software used for RSM modeling. The design matrix was verified experimentally to select the best performing blend. After lyophilization, the dried porous matrices were immersed in methanol for 1 h to induce β-sheet formation and insolubility in water.

2.5 Evaluation of surface texture and pore size

SEM was used to characterize the surface texture of prepared scaffold qualitatively. The samples were sputter coated with gold using Quorum Q150R ES coater and imaged with a Zeiss EVO 18 scanning electron microscope (Zeiss, Germany) using 20 kV accelerating voltage. The pore sizes of scaffolds were analyzed from SEM image using Image J.

2.6 Mass loss study

Biodegradability of synthesized material was investigated in Phosphate buffer saline (PBS) using previously described procedure [14]. Firstly, Scaffold disks of dimension 10 mm were weighed gravimetrically and noted before immersing in PBS. Afterwards, the sample was immersed in PBS at pH 7.4 and incubated at 37 °C for 24 h. At predefined interval, scaffold disks were withdrawn from PBS and dried in hot air oven at 50 °C for 2 days and weighed again. The degradation was obtained using Eq. 1:

$$\text{Degradation } (\%) = \frac{W_o - W_t}{W_o} \times 100 \quad (1)$$

where W_o = Initial dry weight before degradation, W_t = Final dry weight after degradation.

2.7 Swelling study

Swelling of the scaffold was investigated in an aqueous environment. The gravimetric method was used to calculate the swelling. First, dry weights of 10 mm scaffold disks were measured. The test specimens were then immersed in Phosphate Buffer Saline (PBS) at pH 7.4 for 24 h and incubated at room temperature. After 24 h, the disks were withdrawn from PBS, gently wiped with tissue paper to remove extra water and weighed. The Swelling ratio was calculated according to Eq. 2:

$$\text{Swelling } (\%) = \frac{W_s - W_d}{W_d} \times 100 \quad (2)$$

W_s = Weight of swelled disk, W_d = Weight of dried disk.

2.8 Porosity study

The porosity of the silk scaffolds was measured by liquid displacement method [15]. Hexane was used as the displacement liquid as it permeates through silk scaffolds without swelling or shrinking the matrix. The silk scaffold (dry weight, W) was immersed in a known volume (V_1) of hexane in a graduated cylinder for 5 min. The total volume of hexane and the hexane-impregnated scaffold was recorded as V_2. The hexane-impregnated scaffold was then removed from the cylinder, and the residual hexane volume was recorded as V_3. The total volume of the scaffold was calculated using Eq. 3.

$$V = (V_2 - V_1) + (V_1 - V_3) = V_2 - V_3 \quad (3)$$

$V_2 - V_1$ = volume of polymer scaffold, $V_1 - V_3$ = volume of hexane within scaffold, V_1 = known volume of hexane, V_2 = the total volume of hexane and the hexane-impregnated scaffold.

The porosity of scaffold (ε) was obtained by

$$(\varepsilon)\% = \frac{V1 - V3}{V2 - V3} \times 100 \quad (4)$$

V_3 = residual hexane volume after removing hexane-impregnated scaffold.

2.9 *In vitro* studies

2.9.1 Chloramphenicol loading and in vitro release

An antibiotic chloramphenicol (CHL) was loaded by adsorption, allowing sufficient time for adsorbed drug to penetrate into the polymeric scaffold. 10 mm circular disks were carved from the scaffolds and weighed. The sample disks were then immersed in 25 ml of drug-10% ethanol solution (50 mg/ml) in sealed Eppendorf tube and kept for 3 days at room temperature without shaking. At the end of 3 days, the drug loaded samples were taken out, dried at room temperature and used for *in vitro* drug release studies. The relative amount of CHL loaded on to scaffold was calculated by using Eq. 5:

$$\text{Drug loading } (\%, w_t/w_t) = \frac{m_1}{m_2} \times 100\% \quad (5)$$

where m_1 and m_2 are the mass of the drug loaded on the scaffold and a total weight of drug-loaded scaffold respectively.

The *in vitro* drug release was studied for drug loaded Xa, SFX55, and SF scaffolds. The circular scaffold disks were placed into a conical flask containing 50 ml of PBS, pH 7.4 at 37 °C in an orbital shaker at 310 rpm and sink condition was maintained throughout the release experiment. At the pre-determined time interval, an aliquot of 1 ml was withdrawn, while an equal amount of fresh buffer solution was added back to the incubation media. The CHL concentration was determined by UV–Vis spectrophotometer at $\lambda = 288$ nm. All the drug release experiments were carried out in triplicate and data reported as mean ± SD

2.10 Determination of drug release mechanism

2.10.1 Mathematical modeling

The mass transfer mechanism governing the release of the antibiotic from the scaffold was elucidated by fitting experimental data to various mathematical models. The purpose of mathematical modeling was to gain insight into the release mechanism of the specific material system. Drug diffusion, polymer swelling, and polymer erosion are the most important physicochemical phenomena described by zero-order model, the first order model, Higuchi's square root model, Hixson–Crowell model and Korsmeyer–Peppas model [16].

$$\text{Zero-order Model: } F = K_o t \tag{6}$$

$$\text{First Order Model: } \ln(1 - F) = -k_1 t \tag{7}$$

$$\text{Higuchi Model: } F = k_H t^{1/2} \tag{8}$$

$$\text{Hixon}-\text{Crowell Model: } 1 - (1 - F)^{1/3} = k_{1/3} t \tag{9}$$

$$\text{Korsmeyer}-\text{Peppas Model: } F = k_{K-P} t^n \tag{10}$$

where F denotes cumulative fraction (it corresponds to M_t and M_∞, where M_t and M_∞ denotes the absolute cumulative amount of drug released at any time t and at infinity respectively) of drug release at time t. k_0, k_1, k_H, $k_{1/3}$, and k_{K-P} are the apparent release rate constants of the respective mathematical models. The value of exponent n in the Korsmeyer–Peppas model indicates the mechanism of drug release. $n \leq 0.45$ corresponds to a Fickian diffusion (case I transport), $0.45 < n \leq 0.89$ to an anomalous (non-Fickian) transport, $n = 0.89$ to a zero-order (case II) release kinetics, and $n > 0.89$ to a super case II transport. Case II and super case II transports indicate involvement of polymer chain relaxation and erosion in drug release [16].

2.11 Statistical modeling and optimization studies

2.11.1 Design of experiments and response surface methodology

Based on the preliminary experimental studies, a faced centered central composite design (FCCD) was used to investigate the main effects and interactions of independent variable blending ratio, porosity and percentage swelling of scaffold on dependent variable cumulative percent release (CPR). Table 1 represents independent variable, blending ratios and its corresponding composition in the composite scaffold. The independent variables with their coded and actual values are presented Table 2. MATLAB (R 2012a, MathsWork) was used to generate and evaluate design of experiment matrix and for multiple response surface optimizations. The experimental data of dependent variable was fitted to second-order polynomial equation as follows:

$$Y = \beta_o + \sum_{i=1}^{3} \beta_i X_i + \sum_{i=1}^{3} \beta_{ii} X_i^2 + \sum_{i=1}^{3} \sum_{j=1}^{3} \beta_{ij} X_i X_j \tag{11}$$

where Y is the predicted response, β_o, β_i, β_{ii} and β_{ij} are regression coefficients, Xi and X_j are individual effects of dependent variables, X_i^2 are polynomial terms of individual effects, $X_i X_j$ is the interaction effects. One way ANOVA was applied to estimate the significance of RSM model ($p < 0.05$).

2.11.2 Artificial neural network modeling

Artificial neural network (ANN) is biologically inspired computational model which mimics the functioning of human brain to learn certain relationship between input and output parameters through experience [17]. This is a model independent method used to predict complex and non-linear system. For more details about ANN please refers to supplementary Section 1S.

In the present work, a feed forward back propagation neural network was constructed to map the relationship between the three input variables (X_1, X_2, and X_3) and one output variables (CPR). The network architecture is as:

Table 1 Blending ratios and their corresponding composition in the composite scaffold used for design of experiment and response surface methodology (calculated on the basis of composition of silk fibroin in 100 ml of blending solution)

Blending ratio (SF/Xa)	Corresponding coded blend composition
80/20	0.8
50/50	0.5
20/80	0.2

Table 2 Independent variables in the faced type central composite design along with their coded values and levels

Independent variables	High (+ 1)	Low (− 1)
Blend combination (X_1)	0.8	0.2
Porosity (X_2)	67	33
Swelling (X_3)	1248	932

Input layer, one hidden layer with sigmoid transfer function, one output layer with purelin transfer function and one output (Supplementary item, Figure 1S). This network was simulated with the same set of data which was used for RSM. The input along with output dataset was categorized into three sets: Training (16), Validation (4) and Testing (4). The network was trained multiple times by adjusting the number of neurons in the hidden layer and by applying Levenberg–Marquardt learning rule unless the network achieves desired level of accuracy. The network performance was monitored through performance plot, regression analysis option provided in the Neural Network Toolbox of MATLAB 2012a.

2.12 Statistical analysis

The performance and prediction efficiency measured through Mean Square Error (MSE) and Mean Absolute Percentage Error (MAPE) given as

$$\mathrm{MSE} = \frac{1}{n}\sum_{n=1}^{n}(Yn, ANNpredicted - Yn, observed)^2 \qquad (12)$$

$$\mathrm{MAPE} = \frac{100}{n}\sum_{i=1}^{n}|Yi, observed - Yi, predicted/Yi, observed| \qquad (13)$$

The coefficient of determination (R^2) and absolute average deviation (AAD) was used to compare predicted response obtained from RSM and ANN. AAD measured the deviation of predicted data from experimental and was determined using eq

$$\mathrm{AAD} = \frac{1}{n}\left[\sum_{i=1}^{n}|Yi, predicted - Yi, observed)/Yi, observed|\right] \times 100 \qquad (14)$$

where n is the number of observation, Yi, predicted is the predicted response from neural network and RSM respectively and Yi, observed is the actual response.

3 Results

3.1 Optimization through response surface methodology

Blending ratio, porosity, and swelling percentage were chosen for optimization and understanding of their interactive effect on drug release through RSM. The process variable along with experimentally determined values, RSM predicted, and ANN predicted data are presented in Table 3. The RSM predicted CPR values from fabricated scaffold ranged from 46.52 to 64.89%. The RSM predicted maximum response was observed at center point (blending ratio 50/50, porosity 50% and swelling 1090% and minimum were found at run order 2 (blending ratio 20/80, porosity 33% and percent swelling 1248%).

The RSM generated second order polynomial models were applied to calculate the predicted response. The fitted model for cumulative percentage release of antibiotic in coded form is given as:

$$\mathrm{CPR} = 64.89 + 11.91X_1 + 4.27X_2 + 2.61X_3 + 2.19X_1X_2 + 2.06X_1X_3 + 1.42\ X_2X_3 - 0.55X_1X_1 - 2.11X_2X_2 - 0.83X_3X_3 \qquad (15)$$

The adequacy and statistical significance of the model thus obtained was evaluated by ANOVA (Table 4). The high F-value (41.67) and extremely low p value (0.000000014) indicated the significance of model in predicting the percent release at 95% confidence level ($p < 0.05$). The goodness of fit of the model was evaluated through coefficient of determination (R^2). A R^2 value close to unity indicates high degree of association between the experimental and predicted values. The observed R^2 (0.964) values of the model suggest that the regression model could account for 96% of the variability and only 4% of the variability could not be explained by the model [18]. The R^2 value was also in reasonable agreement with the adj. R^2. Furthermore, Durbin–Watson test (dw stats) was also carried out to rule out the possibility of any autocorrelations among residuals. An autocorrelation among residuals can yield high value of R^2 even for poorly fitted models. The results of Durbin–Watson test (dw stats) gave insignificant p value 0.433 at 95% confidence level. An insignificant p is desirable because it implied that the residuals are uncorrelated and indicated goodness of model in predicting the desirable response [19]. The significance of regression coefficient was tested by t test. The t test indicated that the squared term in the regression model are insignificant ($p > 0.05$) and have no effect on the CPR.

Table 3 Faced centered CCD design with independent variables and experimentally determined observed response, predicted response values by RSM and ANN for cumulative percent release

Run order	X_1	X_2	X_3	Experimental cumulative percent release (CPR)	RSM predicted	ANN predicted
1	− 1	− 1	− 1	47.2	48.26	47.50
2	− 1	− 1	1	48.125	46.52	48.36
3	− 1	1	− 1	51.875	49.57	53.05
4	− 1	1	1	54.375	53.53	55.81
5	1	− 1	− 1	63.71	63.56	63.49
6	1	− 1	1	68.76	70.07	68.68
7	1	1	− 1	73.05	73.66	73.12
8	1	1	1	87.93	85.87	83.75
9	− 1	0	0	48.75	52.42	48.91
10	1	0	0	75.98	76.24	77.71
11	0	− 1	0	59.13	58.49	59.25
12	0	1	0	62.48	67.05	65.31
13	0	0	− 1	60.69	61.44	58.59
14	0	0	1	63.48	66.67	63.65
15	0	0	0	65.68	64.89	65.78
16	0	0	0	65.68	64.89	65.78
17	0	0	0	65.68	64.89	65.78
18	0	0	0	65.68	64.89	65.78
19	0	0	0	65.68	64.89	65.78
20	0	0	0	65.68	64.89	65.78
21	0	0	0	65.68	64.89	65.78
22	0	0	0	65.68	64.89	65.78
23	0	0	0	65.68	64.89	65.78
24	0	0	0	65.68	64.89	65.78

3.2 ANN modeling

An ANN model was developed to capture the non-linear effect of blending ratio, swelling, and porosity on CPR. The precise number of neurons to train ANN network was determined through trial and error method. The network topology of 3-10-1 was found to be optimum. The network performance and prediction efficiency were measured through MSE and MAPE, which were 2.5 and 0.94% respectively. A small value of MSE and MAPE is desirable for efficient performance of neural model. The network performances were further authenticated by performance plot (supplementary file, Figure 2S). The regression analysis for all the three training, validation and testing stage confirms excellent performance of neural model (Fig. 1). The ANN predicted CPR ranged from 47.5 to 83.5%. The minimum was observed at run order 1(blending ratio 20/80, porosity 33% and swelling 932%) whereas maximum was observed at run order 8 (blending ratio 80/20, porosity 67%, swelling 1248%).

3.3 Experimental verification of predictive model

Three runs, suggesting maximum, medium and minimum release were selected for experimental verification of models. Three scaffolds of respective blends SFX28, SFX55 and SFX82, were fabricated and their swelling and porosity characteristics were determined.

3.3.1 Swelling

Figure 2A shows the equilibrium swelling of various drug loaded composite scaffolds. The observed swelling was 1248 ± 30, 1090 ± 6 and 932 ± 9% for SFX82, SFX55 and SFX28 scaffold respectively. SFX82 scaffold showed the highest swelling whereas SFX28 exhibited lowest swelling percent. Swelling studies indicated that the drug loaded scaffold attained equilibrium swelling after being immersed in PBS for 24 h. Percent swelling of the entire drug loaded composite scaffold did not exhibit considerable difference afterward till the end of the study (data not shown).

Table 4 Analysis of variance (ANOVA) result

Variable	Cumulative percentage release (CPR)	
	t value	*p value*
X_1	17.100	8.8×10^{-24}
X_2	6.142	2.5×10^{-18}
X_3	3.753	0.002
X_1X_2	2.822	0.013
X_1X_3	2.649	0.019
X_2X_3	1.830	0.088
X_1 X_1	− 0.421	0.679
X_2 X_2	− 1.605	0.130
X_3X_3	− 0.633	0.536
F-stats	41.67	1.4×10^{-22}
Degree of freedom (DF)	14	–

$R^2 = 0.964$

Adjusted $R^2 = 0.940$

Durbin–Watson (dwstats) = 0.433

3.3.2 Mass loss study

Figure 2B shows *invitro* degradation behavior of the composite scaffold in PBS (pH 7.4) after 24 h respectively. The composite scaffold didn't show any loss in mass after 24 h. In fact, mass of the composites increased as manifested by negative weight loss percent. This type of mass loss behavior is characteristic of semi-crystalline polymers like silk. No change in mass of composites was expected because SF is highly resistance to degradation due to its crystalline β-sheet content. The silk fibroin on accounts of its β-crystallite region delays degradation of silk fibroin based material. Hu et al. also observed similar type of degradation for carboxylated agarose/Silk fibroin-Hydroxyapatite composites [14].

3.3.3 Porosity

The porosity percentage and SEM image of porous scaffold are shown in Figs. 2C and 3 respectively. The porosity percentage of SFX82, SFX55, and SFX28 were 67 ± 3, 50 ± 0.5, and 33 ± 1%, respectively. The SEM image show porous structure with uniform distribution of pores and pore interconnection. The variation in porosity and pore interconnection was clearly visible with highest porosity and interconnection observed in SFX82 and lowest in SFX28 composite scaffold respectively. The mean pore size of SFX82, SFX55 and SFX28 calculated from Image J were 58.11, 46.47, 25.30 μm respectively. It was observed that the porosity, pore size and pore interconnection decreases with increase in xanthan content.

3.3.4 In-vitro release study

A model antibiotic, chloramphenicol was loaded on to various composite scaffolds, and *in vitro* release was examined for 120 h (5 days). It was observed that SFX82 and SFX55 gave initial burst release of 73.05 ± 2 and 46.78 ± 17% respectively in the first hour and a maximum of 99 ± 0.4 and 65.68 ± 23% respectively at the end of 120 h (Fig. 2D). After initial burst, the antibiotic was released at controlled rate throughout the study period. On the other hand, release from SFX28 was extremely low with maximum release of 2.14 ± 0.4% throughout the study period. The corresponding drug loading values of composite scaffold for SFX82, SFX55 and SFX28 were 31 ± 0.5, 50 ± 0.01 and 67 ± 0.04 mg respectively.

3.4 Mathematical model fitting of drug release

Only SFX55 was selected for further analysis because it showed low burst release, and better-controlled release rate compared to SFX82 and SFX28 scaffold. To the *in vitro* release data of SFX55, four different drug release model such as Zero order, first order, Higuchi and Korsmeyer–Peppas models were fitted, and the result is presented in Table 5. Zero order and Korsmeyer–Peppas model yielded better fit to the experimental data. The goodness of fit of these models was analyzed through simple linear regression, and appropriate model was selected on the basis of high correlation coefficient (R^2). These models not only gave an insight into the kinetics and mechanism of release, but they can be suitably used for firsthand account of material properties just by fitting release data to model. These insights are helpful in designing optimal polymeric material for drug delivery purposes and provide useful understanding of material performance *invivo*.

4 Discussions

RSM was successfully applied for optimization and prediction of the interactive effect of blending ratio, swelling, and porosity on drug release. It was observed that the RSM model could capture 96% variability in the data. The dependency of drug release (response) on the above mentioned three input variables was studied through contour plots, and results are shown in Fig. 4. The contours showed non-linear relationship between the response variable and the input variables. Figure 4A shows an interactive effect of blend composition and porosity on CPR. At a porosity of 50 ± 0.5%, it can be observed that from right to left, the color of the contour changes rapidly indicating a steep slope, suggesting a substantial change in CPR over a range of blending ratio. This suggested that small change in input

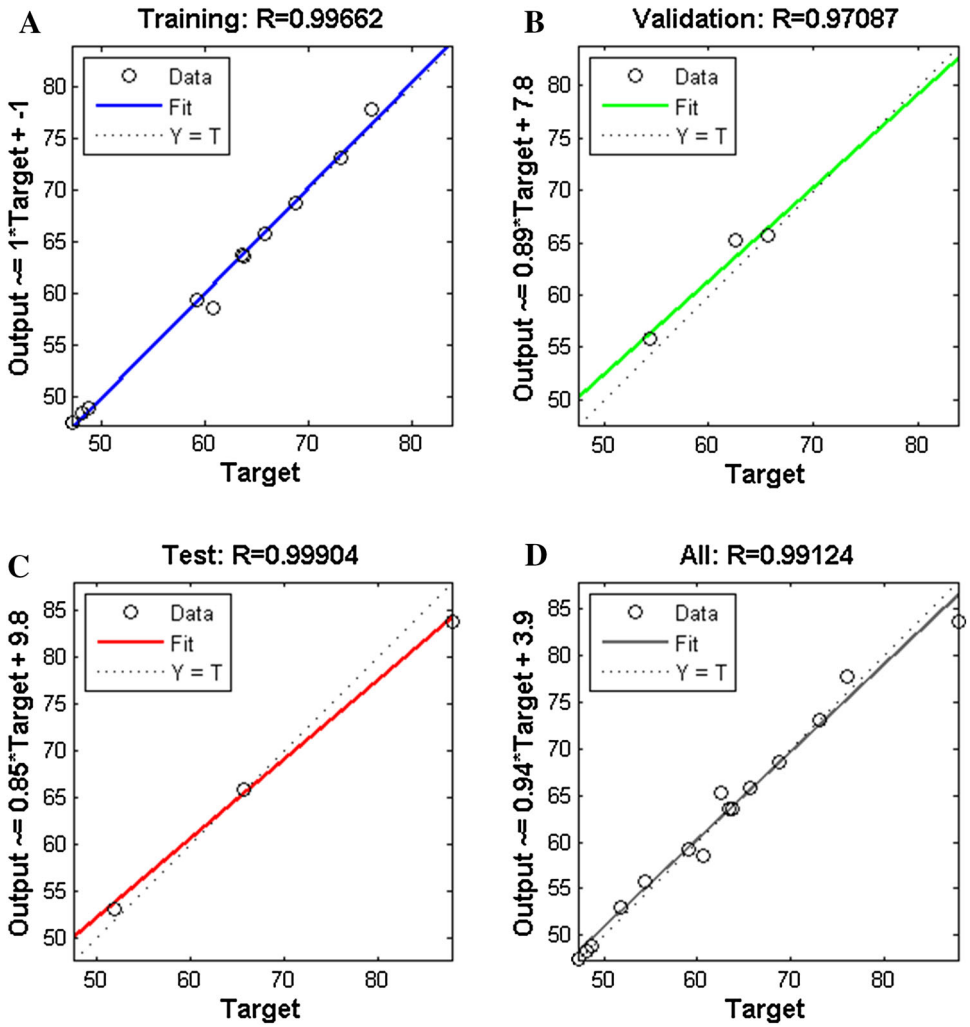

Fig. 1 Regression analysis of ANN model. **A** Training. **B** Testing. **C** Validation phase. **D** Overall

variable can lead to large change in response variable. A similar trend was also observed in contour plot between blend composition and swelling on antibiotic release (Fig. 4B). The slope is much steeper than the slope in Fig. 1A, suggesting that blend composition and swelling of polymeric scaffold have significant effect on CPR. In Fig. 4C, much color change was not observed at central point of swelling, reflecting a small change in release over the range of porosity. It also indicates that swelling in polymer is the dominant factor in case of antibiotic release. The rapid change in contour color indicates non-linear behavior of the process and response variable. The non-linearity of contour arises due to the complexity involved in predicting material properties due to blending. It has been reported that blending changes material composition which affects swelling and porosity of the resulting composite. Therefore, our result of contour plot is in accordance with the literature [20, 21].

4.1 Artificial neural network modeling

ANN is the best choice for capturing non-linear behavior of process variables. A small value of MSE and MAPE (0.94%) and high value of regression analysis (0.991) confirmed an efficient neural model for prediction of responses. MAPE $\leq$ 10% indicates good prediction accuracy [22]. Moreover, the performance plot of the model (Figure 2S) demonstrates decrease in MSE with increase in epoch. The similar characteristic of validation and test curve indicates that no major overfitting occurred. From the graph of actual versus predicted values of CPR, it can be seen that the ANN model developed in this study had a Pearson correlation coefficient (r) of 0.991 which indicate fairly good level of prediction efficiency. It was concluded that the developed ANN model was successful in predicting the CPR with respect to their blending ratio, percentage swelling and porosity at pH 7.4. To the best of our knowledge, this is the first study of its kind that clearly identifies the simultaneous effect of blending ratio, porosity

and percentage swelling on drug release. The developed ANN model has successfully predicted non-linear effect arising out of the parameter used for optimization of drug release.

From Fig. 5, ANN model has higher correlation value than that of RSM model, indicating the success of ANN in better predicting non-linear system. Moreover, AAD values of RSM and ANN model was determined as 2.09 and 0.93% respectively which show greater deviation in RSM prediction than ANN prediction. The result of the entire three criterions: Coefficient of determination (R^2), Pearson Correlation coefficient (r) and AAD inferred that ANN is superior to RSM for prediction and optimization of non-linear system. The superiority of ANN over RSM has been well documented in the literature [23].

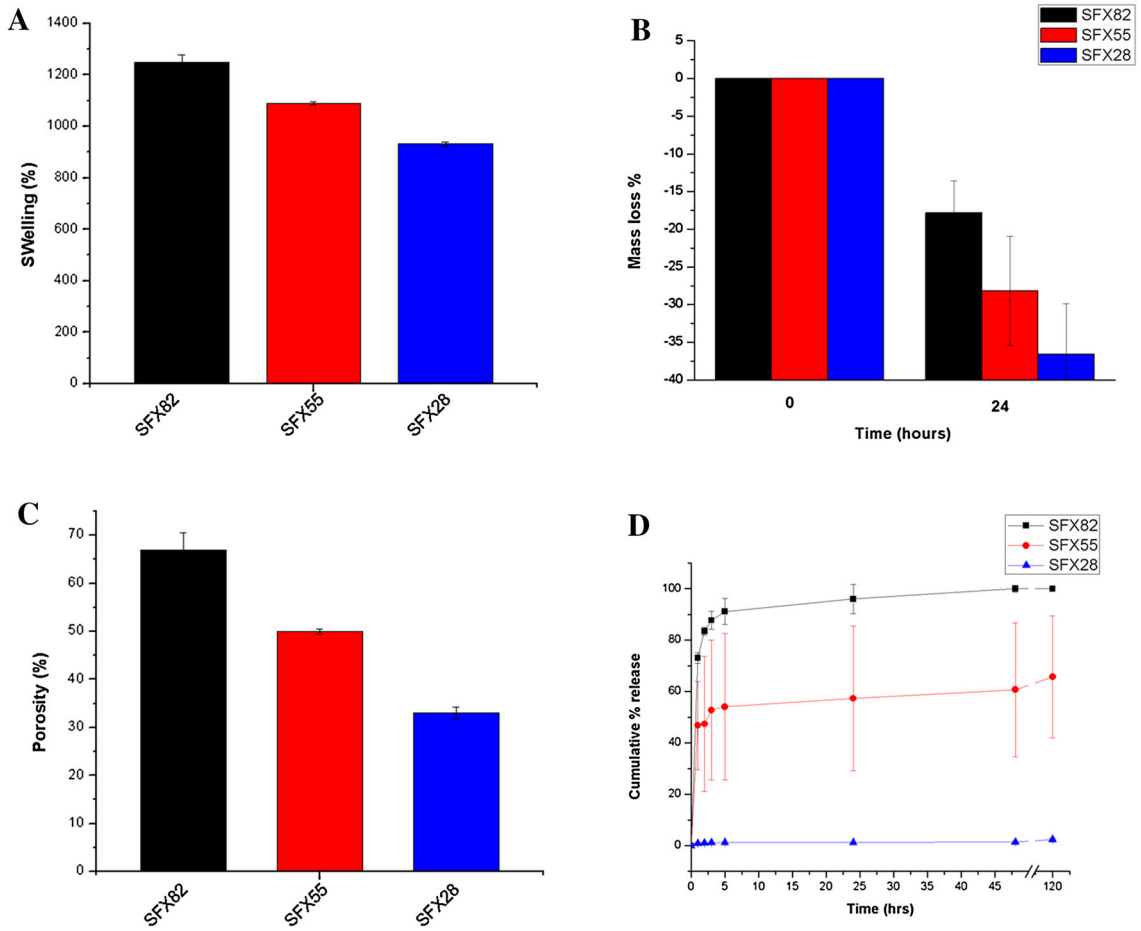

Fig. 2 **A** Swelling profile of SF/Xa composite scaffold in phosphate buffer (pH 7.4) after 24 h. **B** Mass loss % of various scaffold after 24 h. **C** Porosity of various SF/Xa composite scaffolds. **D** *In vitro* drug release behavior of various chloramphenicol loaded SF/Xa composite scaffold (mean ± SD n = 3)

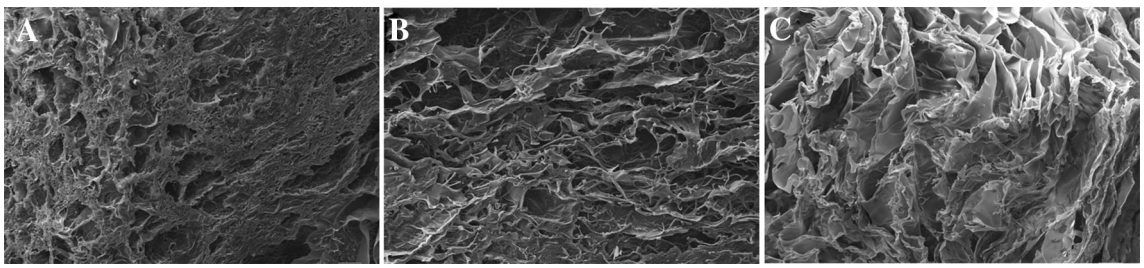

Fig. 3 SEM images of porous composite scaffold. **A** SFX28. **B** SFX55. **C** SFX82 (scale 100 μm)

4.2 *In-vitro* drug release

SFX82 and SFX55 scaffold showed almost identical release profile, but the difference was observed in the amount of released chloramphenicol. The observed burst release was attributed to the dissolution of most accessible drug either from the surfaces or larger pores of the scaffold [24]. After the initial burst, the release rate declines, with maximum release observed for SFX82 and SFX55 as 99 ± 0.4 and 65.68 ± 23% respectively up to 5 days. A clear relation between the content of polymeric blend and drug release rate was observed. With the decreasing SF and increasing xanthan content in the polymer blends, the drug release rate declines. The reduction in release rate was due to hydrophilic nature of Xa. Since Xa can binds a large amount of water and forms a viscous gel structure, which may blockade the pores on the surface of scaffold and restricts the rapid penetration of water in interior of scaffold. Similar explanation was also made to explain controlled and extended release of sodium diclofenac and gentamicin from tamarind seed polysaccharide-alginate composite beads and alginate–calcium phosphate composites respectively [25, 26]. Slow release is beneficial as it aids in controlling and prolonging the antibiotic release. As evident in Fig. 5B, SFX82 released entire antibiotic within 48 h whereas SFX55 has extended-release up to 120 h and still has 35% of drug in the matrix. Such type of biphasic drug release (burst followed by controlled release for prolonged period) is beneficial in application such as wound healing which requires high initial antibiotic

Table 5 Result of mathematical drug release model fitting

Release model	R^2	Adj R^2	n
Zero-order	0.949	0.939	–
First-order	0.316	0.316	–
Korsmeyer–Peppas	0.956	0.947	0.06
Higuchi	0.798	0.798	–
Hixon–Crowell	0.351	0.351	–

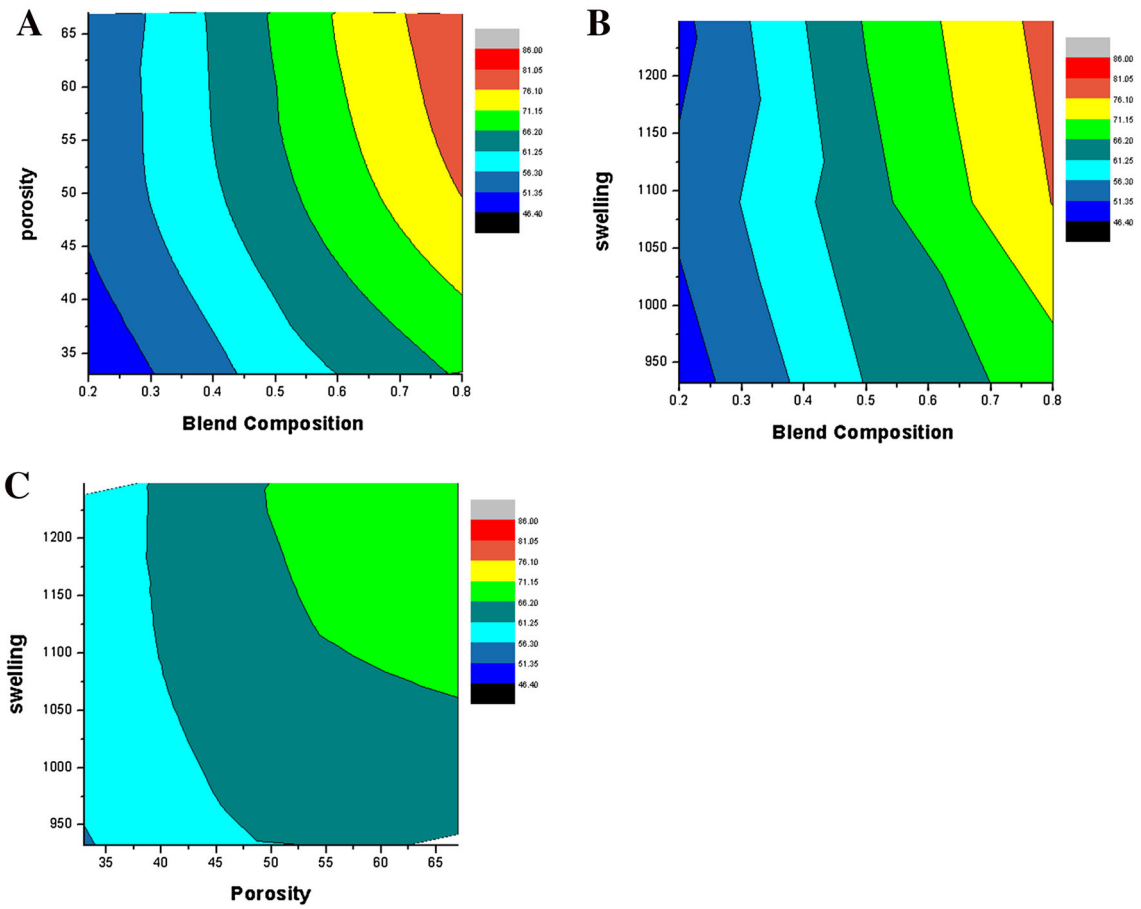

Fig. 4 Contour plots showing effect of independent variables (blending ratios, percent swelling and porosity) on the response variables percentage drug release. **A** Blending ratio versus porosity. **B** Blending ratio versus percent swelling. **C** Porosity versus percent swelling

concentration to control primary infection and less concentration to maintain sanctity of wound for longer period.

Moreover, it was also observed that higher drug loading was obtained as the content of xanthan increased in the composite scaffold. This may be attributed to greater degree of crosslinking between drug and composite scaffold with higher xanthan content. As a result of crosslinking SFX28 also achieved lowest drug release due to tight bounding of drug molecules with matrix.

4.3 Kinetics of chloramphenicol release

Various research in the past have established that the drug release process is dependent on several factors such as method of preparation, porosity and swelling of drug incorporating matrix, drug-material interaction and molecular weight of drug used [25, 27, 28]. These drug release models can give an insight into the drug transport mechanism involved in the release of drug from the scaffold. The comparison of respective R^2 of the various mathematical model yielded that the CHL release followed the zero order Kinetics model ($R^2 = 0.949$) for the period of 120 h. This was further corroborated by fitting the release data with Korsmeyer–Peppas equation. The release data exhibited good agreement with the model giving R^2 values of 0.956 for SFX55 scaffold. The value of release exponent "n" was found to be 0.06, which was less than the value of 0.45. A value $n \leq 0.45$ corresponds to a Fickian diffusion (case I transport), which suggests that release mechanism was controlled by fickian diffusion through the hydrated polymeric matrix [16]. Therefore, it can be concluded that the release of CHL from SFX55 proceeded in a controlled manner and the release mechanism is diffusion controlled.

Another aspect of these mathematical models would be in predicting material properties apart from giving insight into the drug transport process governing the drug release. The knowledge of their limitation and applicability can provide useful insight into the properties of the material. Higuchi model can describe the release when the drug eluting device is non-swollen and non-dissolving [29, 30]; whereas Hopfenberg model describes the release from eroding polymeric system [31] and the Korsemeyer–Peppas model best describes the release from swollen polymeric system [32]. Based on curve fitting results, the Korsmeyer–Peppas model has highest correlation coefficient (R^2) and adjusted R^2 among various model tested, thereby confirming that the material has swollen nature. This was further corroborated by our experimental studies, and it confirmed that SFX55 was a swellable and non-degrading system during the study period (data not shown). Therefore, it can be concluded that the mathematical model gave good approximation of materials properties of the prepared scaffold.

4.4 Effect of swelling on drug release

Swelling behavior of various composite scaffolds was investigated in PBS 7.4. It was observed that as the composition of SF decreases in the SFX82, SFX55 and SFX28 composite scaffold, there was reduction in percentage swelling of scaffold. Blending ratio and degree of cross-linking in polymeric matrix control the swelling behavior. It was reported that high degree of cross-linking causes reduction in swelling [33]. It may be possible that xanthan chains form cross-links with the fibroin chains leading to formation of semi-interpenetrating network which prevents the swelling of scaffold. The cross-linking effect of xanthan was also reported by Lim et al. [34]. Moreover,

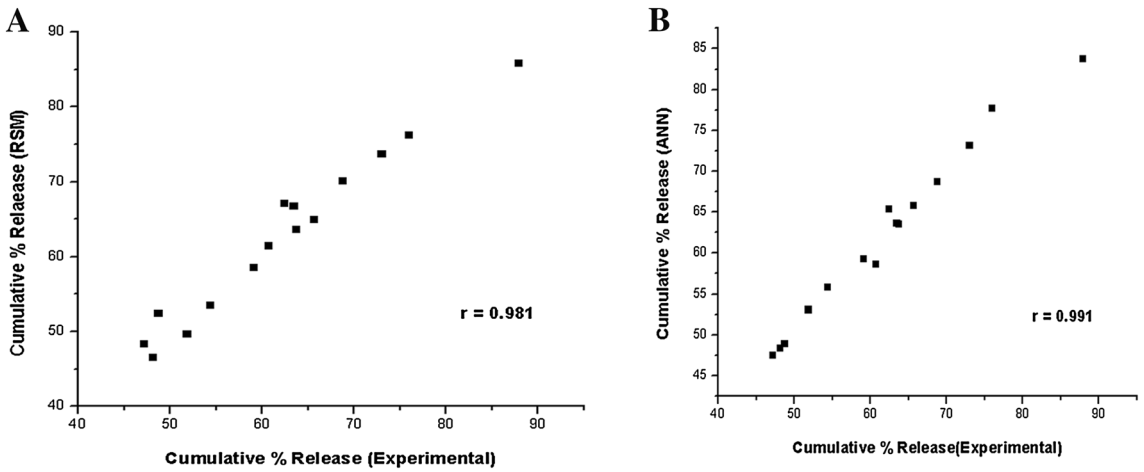

Fig. 5 Pearson correlation analyses between RSM and ANN response and the experimental results. **A** RSM response versus experimental. **B** ANN response versus experimental. (Color figure online)

reduction in swelling due to cross-linking means less surface area is available for release of antibiotic from scaffold. As evident in Fig. 2A, D, composite scaffold with less swelling exhibited reduced drug release rate, apparently suggesting that the release of CHL was controlled by swelling in the composite polymeric blends.

4.5 Effect of porosity on chloramphenicol release

A scaffold must have high porosity, optimum pore size, and interconnected pores size to promote cell growth, nutrient and growth factor delivery, propagation and proliferation. The SFX28, SFX55 and SFX82 scaffold exhibited porosity of 33 ± 1, 50 ± 0.5, and $67 \pm 3\%$ respectively. Cross-linking density influences not only swelling but also has profound effect on porosity. It was reported that polymeric composite with high cross-linking density has lower porosity [35]. The decrease in porosity with increasing xanthan content was due to increase in cross-linking density of the polymeric composite scaffold. The strong cross-links between xanthan and fibroin chains reduce the pore size of scaffold. There is a direct relation between porosity and pore size on drug release, the scaffold with higher porosity and larger pore size shows greater drug release due to penetration of water into the matrix and subsequent dissolution of drug residing into larger pores of matrix [36]. The SFX28 scaffold with minimum porosity and pore size exhibited the lowest release of antibiotic drug due to reduced porosity and pore size.

Acknowledgements The authors are grateful to School of Biochemical Engineering, Indian Institute of Technology (Banaras Hindu University) and Ministry of Human Resource and Development, Government of India, for providing financial support in terms of fellowship, research facilities, and infrastructure for carrying out the present research work.

Compliance with ethical standards

Conflict of interest The authors declare that they have no conflict of interest.

Ethical statements There are no animal experiments carried out for this article.

References

1. Koh L, Cheng Y, Teng C, Khin Y, Loh X, Tee S, et al. Structures, mechanical properties and applications of silk fibroin materials. Prog Polym Sci. 2015;46:86–110.
2. Li ZH, Ji SC, Wang YZ, Shen XC, Liang H. Silk fibroin-based scaffolds for tissue engineering. Front Mater Sci. 2013;7:237–47.
3. Nourmohammadi J, Roshanfar F, Farokhi M, Haghbin Nazarpak M. Silk fibroin/kappa-carrageenan composite scaffolds with enhanced biomimetic mineralization for bone regeneration applications. Mater Sci Eng C Mater Biol Appl. 2017;76:951–8.
4. Zhou J, Zhang B, Liu X, Shi L, Zhu J, Wei D, et al. Facile method to prepare silk fibroin/hyaluronic acid films for vascular endothelial growth factor release. Carbohydr Polym. 2016;143:301–9.
5. Li DW, Lei X, He FL, He J, Liu YL, Ye YJ, et al. International journal of biological macromolecules silk fibroin/chitosan scaffold with tunable properties and low inflammatory response assists the differentiation of bone marrow mesenchymal stem cells. Int J Biol Macromol. 2017;105:584–97.
6. Badwaik HR, Giri TK, Nakhate KT, Kashyap P, Tripathi DK. Xanthan gum and its derivatives as a potential bio-polymeric carrier for drug delivery system. Curr Drug Deliv. 2013;10:587–600.
7. Khan F, Tanaka M, Ahmad SR. Fabrication of polymeric biomaterials: a strategy for tissue engineering and medical devices. J Mater Chem B Mater Biol Med. 2015;3:8224–49.
8. Chamoli S. ANN and RSM approach for modeling and optimization of designing parameters for a V down perforated baffle roughened rectangular channel. Alexandria Eng J. 2015;54:429–46.
9. Zaki MR, Varshosaz J, Fathi M. Preparation of agar nanospheres: comparison of response surface and artificial neural network modeling by a genetic algorithm approach. Carbohydr Polym. 2015;122:314–20.
10. Gubskaya AV, Khan IJ, Valenzuela LM, Lisnyak YV, Kohn J. Investigating the release of a hydrophobic peptide from matrices of biodegradable polymers: an integrated method approach. Polymer (Guildf). 2013;54:3806–20.
11. McGinty S. A decade of modelling drug release from arterial stents. Math Biosci. 2014;257:80–90.
12. Arifin DY, Lee LY, Wang CH. Mathematical modeling and simulation of drug release from microspheres: implications to drug delivery systems. Adv Drug Deliv Rev. 2006;58:1274–325.
13. Abdulkhani A, Daliri Sousefi M, Ashori A, Ebrahimi G. Preparation and characterization of sodium carboxymethyl cellulose/silk fibroin/graphene oxide nanocomposite films. Polym Test. 2016;52:218–24.
14. Hu JX, Ran JB, Chen S, Jiang P, Shen XY, Tong H. Carboxylated Agarose (CA)-Silk Fibroin (SF) Dual Confluent Matrices Containing Oriented Hydroxyapatite (HA) Crystals: Biomimetic Organic/Inorganic Composites for Tibia Repair. Biomacromolecules. 2016;17:2437–47.
15. Kim UJ, Park J, Kim HJ, Wada M, Kaplan DL. Three-dimensional aqueous-derived biomaterial scaffolds from silk fibroin. Biomaterials. 2005;26:2775–85.
16. Muhsin MD, George G, Beagley K, Ferro V, Wang H, Islam N. Effects of chemical conjugation of L-leucine to chitosan on dispersibility and controlled release of drug from a nanoparticulate dry powder inhaler formulation. Mol Pharm. 2016;13:1455–66.
17. Vatankhah E, Semnani D, Prabhakaran MP, Tadayon M, Razavi S, Ramakrishna S. Artificial neural network for modeling the elastic modulus of electrospun polycaprolactone/gelatin scaffolds. Acta Biomater. 2014;10:709–21.
18. Bukzem AL, Signini R, Dos Santos DM, Lião LM, Ascheri DP. Optimization of carboxymethyl chitosan synthesis using response surface methodology and desirability function. Int J Biol Macromol. 2016;85:615–24.
19. Dwtest. http://in.mathworks.com/help/stats/dwtest.html. Accessed 12 May 2017.
20. Bukhari SMH, Khan S, Rehanullah M, Ranjha NM. Synthesis and characterization of chemically cross-linked acrylic acid/gelatin hydrogels: effect of pH and composition on swelling and drug release. Int J Polym Sci. 2015;2015:187961.

21. Takeno H, Kimura Y, Nakamura W. Mechanical, swelling, and structural properties of mechanically tough clay-sodium polyacrylate blend hydrogels. Gels. 2017;3:10.
22. Yadav AK, Malik H, Chandel SS. Selection of most relevant input parameters using WEKA for artificial neural network based solar radiation prediction models. Renew Sustain Energy Rev. 2014;31:509–19.
23. Singh P, Shera SS, Banik J, Banik RM. Optimization of cultural conditions using response surface methodology versus artificial neural network and modeling of l-glutaminase production by Bacillus cereus MTCC 1305. Bioresour Technol. 2013;137:261–9.
24. Cabezas LI, Gracia I, de Lucas A, Rodríguez JF. Novel model for the description of the controlled release of 5-fluorouracil from PLGA and PLA foamed scaffolds impregnated in supercritical CO_2. Ind Eng Chem Res. 2014;53:15374–82.
25. Nayak AK, Pal D. Development of pH-sensitive tamarind seed polysaccharide-alginate composite beads for controlled diclofenac sodium delivery using response surface methodology. Int J Biol Macromol. 2011;49:784–93.
26. Perez RA, Shin SH, Han CM, Kim HW. Bioactive injectables based on calcium phosphates for hard tissues: a recent update. Tissue Eng Regen Med. 2015;12:143–53.
27. Carbinatto FM, de Castro AD, Evangelista RC, Cury BSF. Insights into the swelling process and drug release mechanisms from cross-linked pectin/high amylose starch matrices. Asian J Pharm Sci. 2014;9:27–34.
28. Karuppuswamy P, Venugopal JR, Navaneethan B, Laiva AL, Ramakrishna S. Polycaprolactone nanofibers for the controlled release of tetracycline hydrochloride. Mater Lett. 2015;141:180–6.
29. Dash S, Murthy PN, Nath L, Chowdhury P. Kinetic modeling on drug release from controlled drug delivery systems. Acta Pol Pharm. 2010;67:217–23.
30. Siepmann J, Peppas NA. Higuchi equation: derivation, applications, use and misuse. Int J Pharm. 2011;418:6–12.
31. Fu Y, Kao WJ. Drug release kinetics and transport mechanisms from semi-interpenetrating networks of gelatin and poly (ethylene glycol) diacrylate. Pharm Res. 2009;26:2115–24.
32. Siepmann J, Siepmann F. Fundamentals and Applications of Controlled Release Drug Delivery. In: Siepmann J, Siegel RA, Rathbone MJ, editors. Swelling controlled drug delivery system. Advances in delivery science and technology. New York: Springer; 2012. p. 153–70.
33. Bueno VB, Bentini R, Catalani LH, Petri DF. Synthesis and swelling behavior of xanthan-based hydrogels. Carbohydr Polym. 2013;92:1091–9.
34. Chung HJ, Min D, Kim JY, Lim ST. Effect of minor addition of xanthan on cross-linking of rice starches by dry heating with phosphate salts. J Appl Polym Sci. 2007;105:2280–6.
35. Chavda H, Patel C. Effect of crosslinker concentration on characteristics of superporous hydrogel. Int J Pharm Investig. 2011;1:17–21.
36. Klose D, Siepmann F, Elkharraz K, Krenzlin S, Siepmann J. How porosity and size affect the drug release mechanisms from PLGA-based microparticles. Int J Pharm. 2006;314:198–206.